Moving towards daytime observing at the Large Millimeter Telescope

Schloerb, F. Peter, Souccar, Kamal, Chávez Dagostino, Miguel, Ferrusca Rodriguez, Daniel, Gale, David, et al.

F. Peter Schloerb, Kamal Souccar, Miguel Chávez Dagostino, Daniel Ferrusca Rodriguez, David M. Gale, Arturo Gómez-Ruiz, Andrea Léon Huerta, David H. Hughes, David O. Sánchez-Arguelles, Grant W. Wilson, "Moving towards daytime observing at the Large Millimeter Telescope," Proc. SPIE 11445, Ground-based and Airborne Telescopes VIII, 114455J (13 December 2020); doi: 10.1117/12.2562775

SPIE.

Event: SPIE Astronomical Telescopes + Instrumentation, 2020, Online Only

Moving towards daytime observing at the Large Millimeter Telescope

F. Peter Schloerb[a], Kamal Souccar[a], Miguel Chávez Dagostino[b], Daniel Ferrusca Rodriguez[b], David M. Gale[b], Arturo Gómez-Ruiz[b], Andrea Léon Huerta[b], David H. Hughes[b], David O. Sánchez-Arguelles[b], Grant W. Wilson[a]
[a]Department of Astronomy, University of Massachusetts, Amherst Massachusetts, USA; [b]Instituto Nacional de Astrofísica, Óptica, y Electrónica, Tonantzintla, Puebla, Mexico

ABSTRACT

The Large Millimeter Telescope *Alfonso Serrano* (LMT) is a 50m-diameter radio telescope for millimeter-wave astronomy. In this paper we describe a number of initiatives underway to upgrade the antenna systems and permit scientific observations during daylight hours. We summarize recent efforts to characterize the thermal gradients that occur within the LMT structure and to identify important modes of surface deformation. The mitigation program involves use of the LMT's active surface to counteract the effects of measured thermal gradients within the antenna structure. It also includes active measures such as the installation of a ventilation system in the antenna backup structure. Prospects for additional active metrology measurements of the antenna surface for real-time surface corrections are also discussed.

Keywords: Radio Telescopes, Thermal Behavior of Radio Telescopes, Millimeter-wave Telescopes, Surface Deformation, Thermal Gradients, Thermal Models, Zernike Polynomials, Telescope Design

1. INTRODUCTION

The Large Millimeter Telescope *Alfonso Serrano* (LMT) is a 50m-diameter radio telescope for millimeter-wave radio astronomy (see Figure 1). Heretofore, the antenna has been used for scientific observations almost exclusively during nighttime conditions when thermal gradients within the structure are minimized. Structural temperature gradients lead to deformations of the antenna structure, which in turn translate into degradation of the overall performance of the antenna. Thermally induced deformations, which may lead to errors in the pointing of the telescope beam and to reduction of telescope gain, are often an important limiting factor in the overall performance of a large antenna.

Thermally induced deformation of the LMT structure will, naturally, be a greater problem during daylight hours when the telescope is subject to direct solar heating. Nevertheless, the LMT project seeks to expand use of the telescope into daylight hours in order to increase the amount of science observing time available to our user community. LMT site characteristics, shown in Figure 2, indicate that excellent observing conditions exist during morning hours, and conditions remain useful for observations during the afternoon[1]. Expanding the use of the telescope into daylight hours is also especially advantageous for Very Long Baseline Interferometry observations with the LMT paired with other telescopes over intercontinental baselines. Improved performance of the LMT during daylight hours will extend the lengths of the u-v tracks obtained and improve the overall u-v coverage of VLBI experiments. Finally, strategies that improve the thermal behavior of the telescope under daytime conditions are expected to improve the nighttime performance of the telescope as well.

In this paper, we describe our program for improving the LMT's thermal performance with the goal of achieving useful scientific observations during daylight hours. We will present a brief overview of the telescope design, followed by characterization of the telescope's thermal behavior. Then we will present approaches that are currently in use at the telescope to remove major thermal effects. Finally, we will outline further plans for mitigation of thermal effects, including next steps in the pursuit of a real-time metrology system for measuring structural deformations.

Ground-based and Airborne Telescopes VIII, edited by Heather K. Marshall, Jason Spyromilio, Tomonori Usuda, Proc. of SPIE Vol. 11445, 114455J · © 2020 SPIE
CCC code: 0277-786X/20/$21 · doi: 10.1117/12.2562775

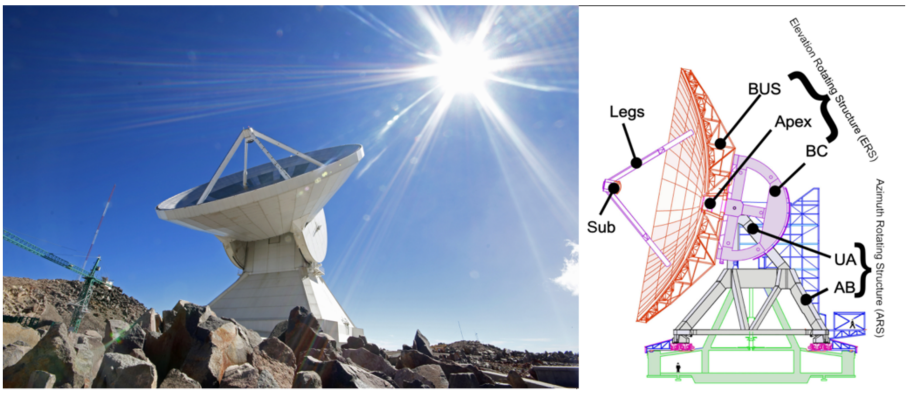

Figure 1. (left) A view of the LMT at its site atop Sierra Negra in the Mexican state of Puebla. (right) Summary diagram identifying major telescope structural components described in the text. The antenna is a wheel-on-track structure with an Azimuth Rotating Structure (ARS) which rotates in azimuth and an Elevation Rotating Structure (ERS) which moves in elevation. The ARS has two steel substructures which are referred to in the text: the Alidade Base (AB) and the Upper Alidade (UA). The ERS has a number of components as well. The antenna Backup Structure (BUS) is a steel truss structure that supports the reflector surface segments. The BUS is balanced by a pair of counterweights (BC). The BUS is built around a steel hub, which is known as the Apex Cabin (Apex). Finally, the secondary mirror (Sub) is supported by a set of four beams, known as the tetrapod (Legs).

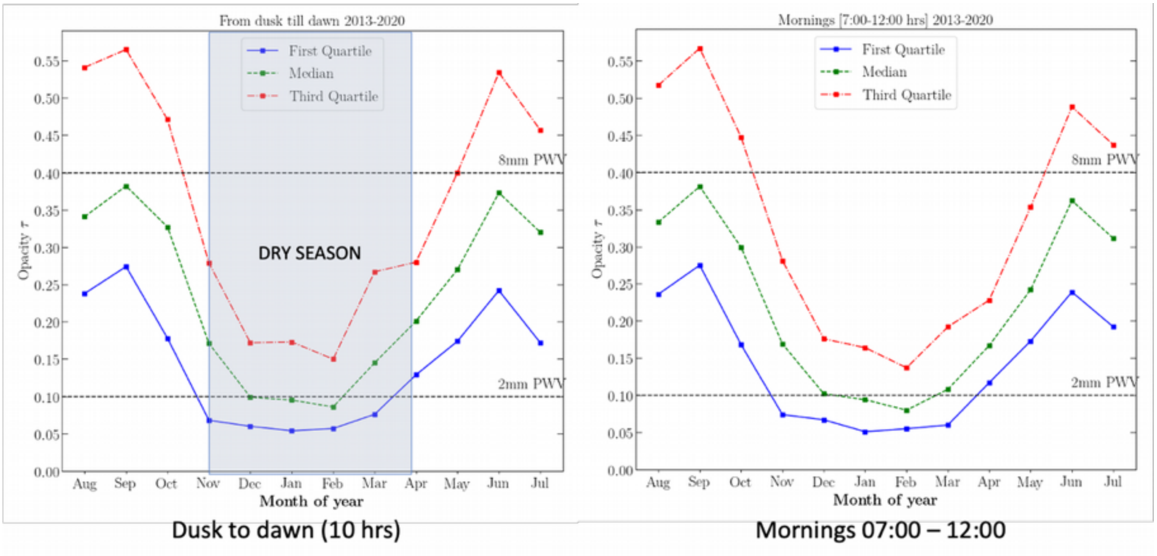

Figure 2. (left) Measured opacities at 225 GHz at the LMT site under nighttime conditions. Opacities corresponding to the first quartile, median, and third quartile are indicated. The site is a seasonal site with a winter dry season which provides excellent observing conditions with median opacities of ~2mm precipitable water vapor. (right) Opacity values at the LMT site during morning hours. The morning values of opacity are essentially the same as the night conditions, implying that daytime observing can be scientifically productive.

2. THERMAL BEHAVIOR OF THE LMT

2.1 LMT Thermal Design

The original designers of the LMT (formerly MAN Tecnologie, now MT Mechatronics) considered the impact of thermal gradients within the structure. The major structural components of the LMT are identified in Figure 1, and the antenna designers computed expected thermal distortions that might arise due to temperature differences between components.

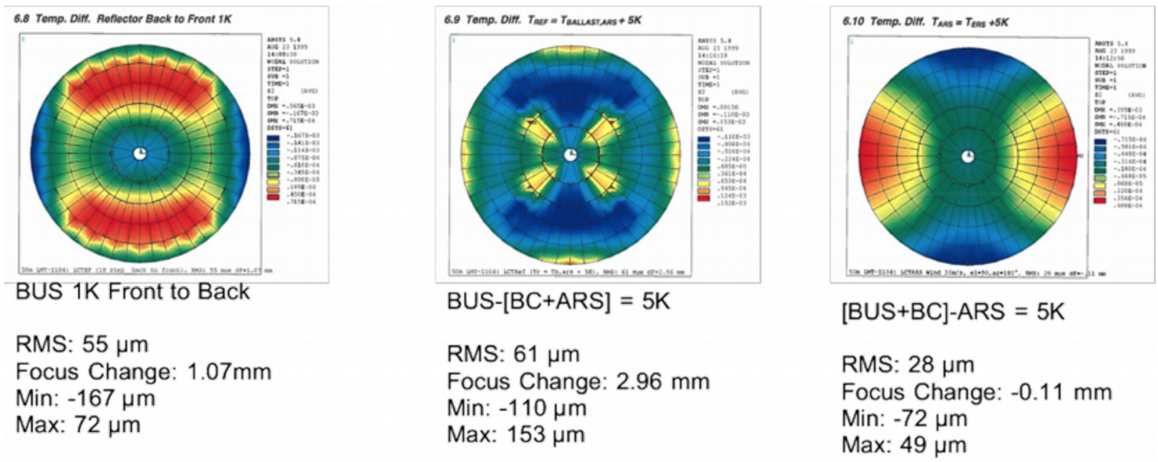

Figure 3. Finite element model predictions of deformations in response to temperature differences within the LMT structure. Three thermal cases are shown: (left) a 1 K gradient between the front-to-back of the antenna backup structure (BUS); (middle) a 5 K difference between the antenna backup structure (BUS) and the antenna counterweights (BC) and alidade (ARS); and (right) a 5 K difference between the entire structure rotating in elevation (ERS, which includes the BUS and the counterweights) and the azimuth rotating structure (ARS).

Figure 3 shows the predicted deformations for three thermal cases in the original design study: [1] a 1 K gradient between the front-to-back of the antenna backup structure (BUS); [2] a 5 K difference between the antenna backup structure (BUS) and the BUS counterweights (BC) and azimuth rotating structure (ARS); and [3] a 5 K difference between the entire structure rotating in elevation (ERS, which includes both the BUS and its counterweights) and the azimuth rotating structure (ARS). The predictions of the thermal model show that small (1 K) gradients in the BUS are much more important than larger differences (5 K) between the main structural components. Because of this, the antenna design included specification of an active ventilation system for the BUS which was intended to minimize temperature gradients. Though this system has yet to be added, it is an important part of our overall plan to improve the telescope's thermal behavior.

2.2 Structural Temperatures

The LMT has a set of temperature sensors located at many positions on the structure to allow measurements of the temperature gradients that develop as the structure is heated and cooled over the full 24-hour diurnal cycle. In Figures 4 and 5 below we show results for a period of a few days when the diurnal cycle of local air temperature was consistent from day to day. During this time interval, the antenna was primarily pointed at the north horizon. However, at mid-morning and midafternoon, the telescope was sometimes pointed to the zenith position for maintenance. A history of the antenna movements is shown in the plots along with the structural temperatures.

Figure 4 shows the temperatures measured for several of the components identified in Figure 1. Many general features of the antenna's thermal response are apparent. For the massive structural components, including alidade, BUS counterweights (BC) and inner hub of the BUS (Apex), the components have an amplitude close to the ambient air temperature with a phase lag of a few hours. Within the backup structure, we have presented the temperatures at three radial positions corresponding to locations at approximately ¼, ½, and ¾ of the dish radius. The observed behavior is interesting because of the relative amplitudes and phase shifts between the different radial positions. Differences in the thermal mass of the steel structural elements of the BUS leads to the development of temperature differences within the BUS. Finally, in the lower right panel, we show the temperatures of the subreflector support legs and the subreflector mounting point at the peak of that structure. These structures are all in the open air and exposed to sunlight, resulting in significant heating during the daytime.

2.3 Temperature Differences within the Antenna Structure

The left panel of Figure 5 shows the temperature differences observed between a number of the heavy structural components of the telescope. We note systematic, but small, temperature differences arise between the alidade structure

(ARS) and large counterweights (BC) and the steel structure (Apex) that is the hub of the antenna backup structure. To characterize differences between the BUS and the large steel elements, we also show the difference between the average temperature at a point in the BUS approximately halfway between the center of the primary mirror and its edge (labelled "Mid"). Again, it may be noted that systematic changes occur during the day, but the magnitude of the changes is small compared to the structural thermal cases presented in Figure 3.

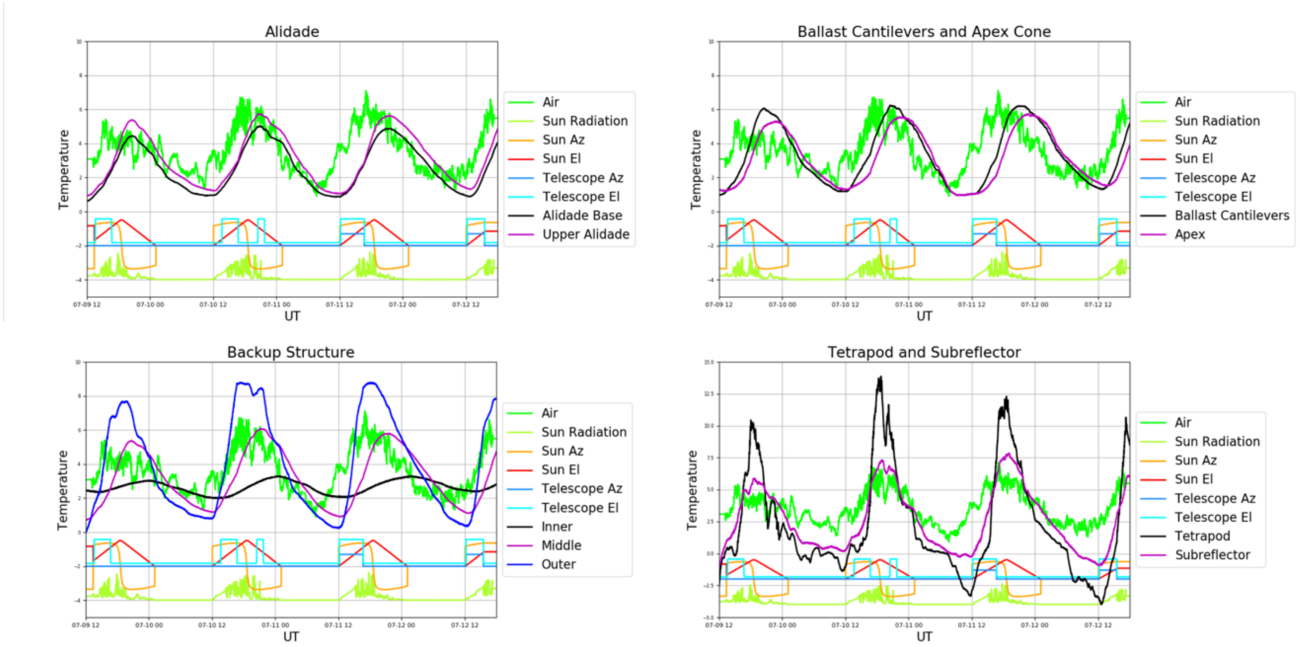

Figure 4. Temperatures of LMT structural elements. (upper left) Temperatures of the alidade compared to ambient outside air temperature. (upper right) Temperatures of the BUS counterweights (labeled "Ballast Cantilevers") and the central hub structure of the antenna backup structure (Apex). (lower left) Temperatures at different radial positions within the BUS. (lower right) Temperatures of the secondary support legs (tetrapod) and the secondary position. Curves at the bottom indicate the azimuth (orange) and elevation (red) of the Sun and the amount of solar radiation incident on the site as measured by a sensor on the site weather station (green). The telescope position is indicated in blue lines.

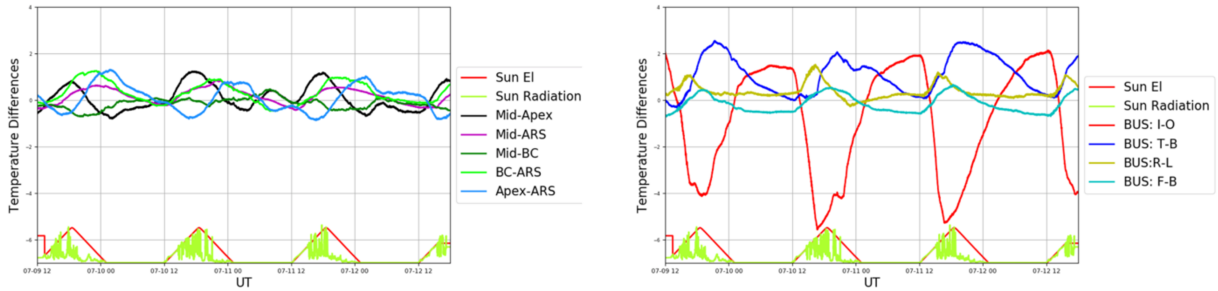

Figure 5. (left) Temperature Differences between structural elements of the LMT. "Mid" refers to the average value of the BUS at a location approximately half the distance from center of the primary mirror to its edge. The "Apex", "BC", and "ARS" components are identified in Figure 1. (right) Temperature Differences between structural elements within the backup structure (BUS) of the LMT. The differences Inner-Outer (I-O), Top-Bottom (T-B), Right-Left (R-L), and Front-Back (F-B) are shown in the figure. Curves at the bottom indicate the elevation of the Sun (red) and the amount of solar radiation incident on the site as measured by a sensor on the site weather station.

While the left panel of Figure 5 illustrated that temperature differences between the major structural elements of LMT tended to be small, we note that the same statement cannot be made about temperature gradients within the BUS. The right panel shows temperature differences measured between the different regions within the BUS. We form averages of all sensors located: [1] in an inner ring of sensors (I) located about 7m from the center; [2] in an outer ring of sensors (O) located about 5m from the edge of the dish; [3] in the top half of the BUS (T), where top is defined according to position when the antenna is pointed to the horizon ; [4] in the bottom half of the BUS (B); [5] in the right half (R), as viewed from in front of the antenna; [6] in the left half (L); [7] on the front chord of the BUS structure closest to the surface (F); and on the back chord (B). The differences Inner-Outer (I-O), Top-Bottom (T-B), Right-Left (R-L), and Front-Back (F-B) are shown in the figure.

Since the thermal case from the LMT design study found significant deformations with only a 1-degree difference between front and back chords in the BUS, it is notable that larger differences exist. The observed differences are accounted for in a straightforward manner. The large temperature difference between the inner and outer parts of the BUS primarily reflects the different thermal mass in the BUS's structural elements. Right-Left and Front-Back gradients reflect uneven solar heating during the day. The Top-Bottom temperature difference, which leads to the second largest gradient observed, partly reflects uneven solar heating but also is a response to trapping of hot air in the upper part of the BUS.

2.4 Temperature Measurements within LMT Surface Segments

Finally, we present a set of measurements of the structural elements within the surface segments themselves. These temperature sensors are not a part of the regular complement of sensors on the telescope and represent results of individual experiments. The goal of the work was to see how solar heating affected the temperature of the surface of the reflector panels and determine whether temperature gradients were introduced into the segment structure during the day.

Figure 6 shows the main structural components of a segment and presents a set of temperature measurements carried out in March 2012 at full scale. The surface reflector panels get very hot (50 C or greater) under solar illumination but are insulated so that the temperature of the structures below is not strongly affected. The baseplate and subframe structures converge on the BUS air temperature during the night but differ by 2-3 degrees from one another during the day. The temperature of the BUS truss follows the air temperature with a small phase lag. We note that design studies of the segments showed that the large temperature difference between the surface subpanels and the rest of the structure did not greatly affect the precision of the subpanels or their alignment. Thus, we anticipate that the segments will perform well even in the presence of large differences between the surface subpanels and the rest of the segment structure.

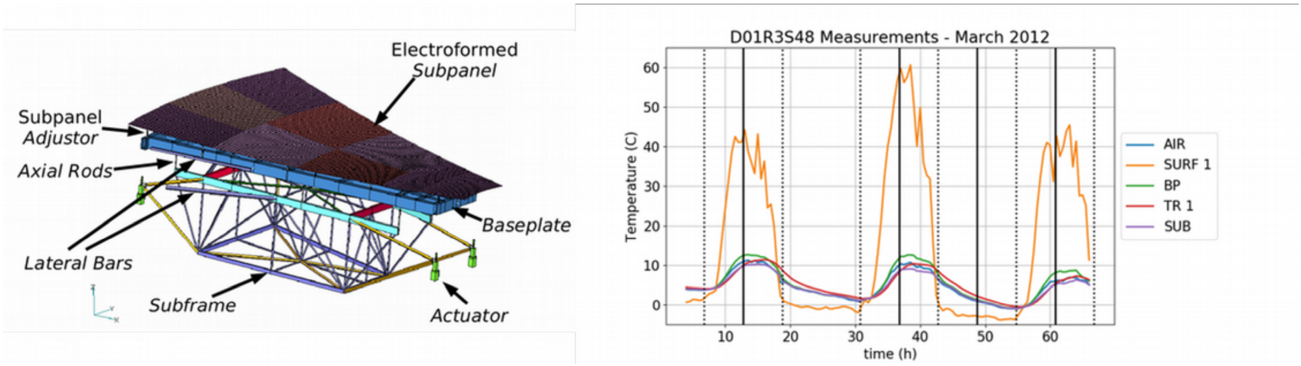

Figure 6. (left) Identification of the structural elements in an LMT surface segment; (right) measurements of temperature of some structural elements and the local air temperature. The curve labelled "SURF 1" shows the temperature of the surface. The LMT's precision surface panels get very hot in response to solar heating that occurred during daytime. Other structural temperatures include the baseplate (BP), which supports the subpanels, and the segment subframe structure (SUB), which attaches to the BUS and supports the subpanel/baseplate unit. Finally, temperatures were obtained for the top-chord beam (TR 1) of the BUS. Noon is indicated on the plot with a vertical black line, with sunrise and sunset indicated with vertical dotted lines.

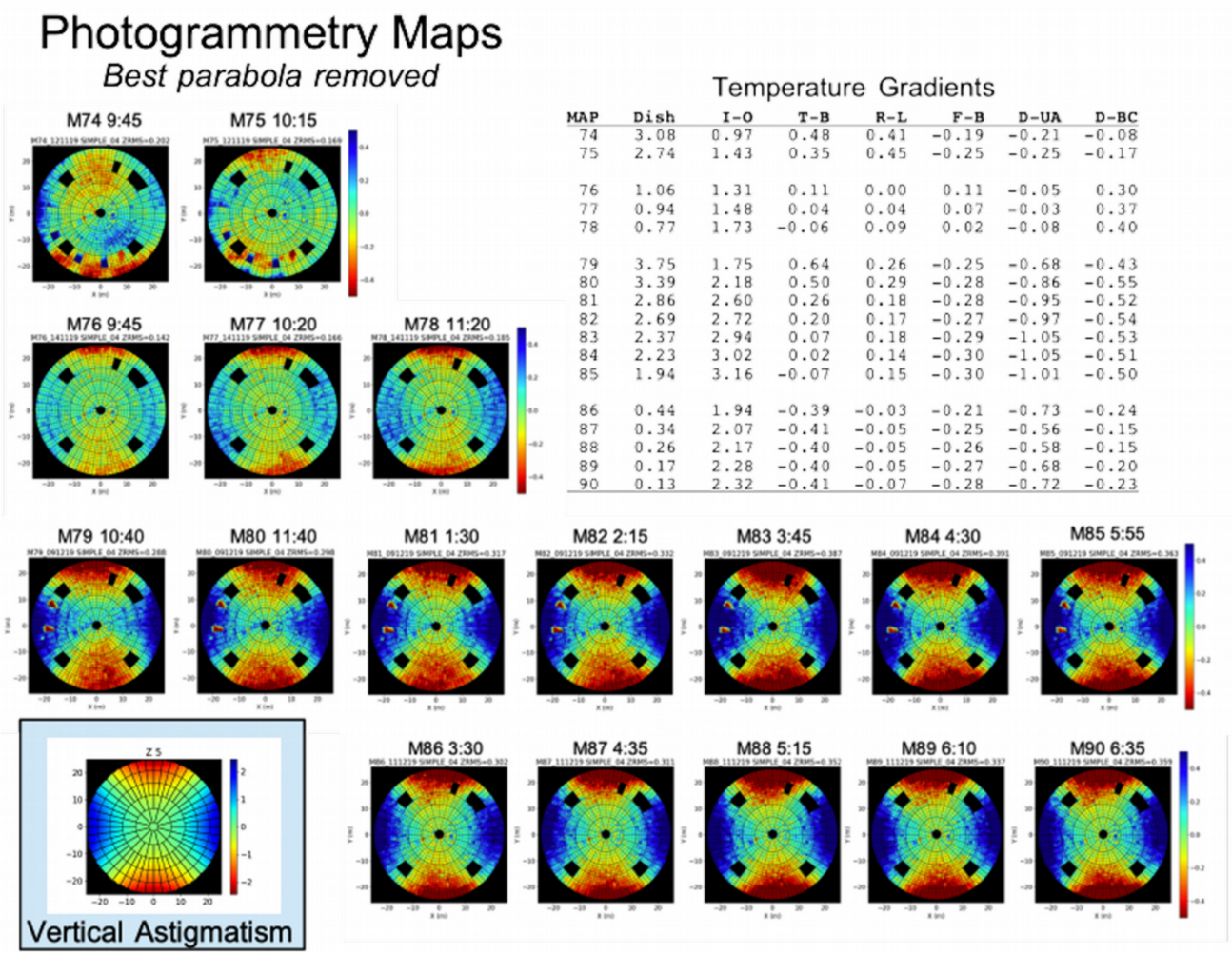

Temperature Gradients

MAP	Dish	I-O	T-B	R-L	F-B	D-UA	D-BC
74	3.08	0.97	0.48	0.41	-0.19	-0.21	-0.08
75	2.74	1.43	0.35	0.45	-0.25	-0.25	-0.17
76	1.06	1.31	0.11	0.00	0.11	-0.05	0.30
77	0.94	1.48	0.04	0.04	0.07	-0.03	0.37
78	0.77	1.73	-0.06	0.09	0.02	-0.08	0.40
79	3.75	1.75	0.64	0.26	-0.25	-0.68	-0.43
80	3.39	2.18	0.50	0.29	-0.28	-0.86	-0.55
81	2.86	2.60	0.26	0.18	-0.28	-0.95	-0.52
82	2.69	2.72	0.20	0.17	-0.27	-0.97	-0.54
83	2.37	2.94	0.07	0.18	-0.29	-1.05	-0.53
84	2.23	3.02	0.02	0.14	-0.30	-1.05	-0.51
85	1.94	3.16	-0.07	0.15	-0.30	-1.01	-0.50
86	0.44	1.94	-0.39	-0.03	-0.21	-0.73	-0.24
87	0.34	2.07	-0.41	-0.05	-0.25	-0.56	-0.15
88	0.26	2.17	-0.40	-0.05	-0.26	-0.58	-0.15
89	0.17	2.28	-0.40	-0.05	-0.27	-0.68	-0.20
90	0.13	2.32	-0.41	-0.07	-0.28	-0.72	-0.23

Figure 7. Photogrammetry maps of LMT surface over four nights of measurements. Observations were made with the telescope fixed at an elevation of 62 degrees and no changes were made to the active surface between the maps. In all cases, the surface has had a best fitting parabola removed from the measurements. Each map has the local time indicated. The maps show clear changes in the surface from night to night and during the night. The vertical color scale is +/- 0.5 mm. The most obvious feature of the deformation is well modeled by an astigmatism (compare maps to a picture of the Zernike vertical astigmatism polynomial in the lower left corner of the figure.)

3. MEASUREMENT OF SURFACE DEFORMATIONS AT LMT

3.1 Observations

The LMT uses a photogrammetry system for the purpose of measuring and setting the antenna surface[2]. Ideally one would make measurements during the night after the antenna has had an opportunity to stabilize its temperature. However, looking at Figures 4 and 5, it is clear that the temperatures within the structure continue to change during the night, and in the course of making regular photogrammetry measurements, we have found that the shape of the surface changes during the night and from night-to-night. Figure 7 presents a summary of surface maps obtained on four different nights at the LMT. Each photogrammetry map takes 30-45 minutes to make. In this set of measurements, maps are made sequentially at a single elevation without making any adjustments to the shape of the primary using the LMT's active surface. The photogrammetry point cloud is fit to a best paraboloid and the maps presented here show the residuals to that fit. It is clear that a large deformation which follows the Zernike vertical astigmatism polynomial is a major variable feature in the

maps. This is not altogether surprising since astigmatism is often one of the leading thermal deformation shapes in antenna structures. However, at this time we have not associated the feature with a specific thermal condition at the LMT.

3.2 Analysis

In addition to visual inspection of the maps in Figure 7, it is useful to attempt a quantitative analysis of the LMT's surface deformations. We have accomplished this by fitting the photogrammetry point cloud to a model that characterizes surface deformations in terms of Zernike polynomials. For each map, we fit a sequence of Zernike models of increasing order to the data. This allowed estimation of the coefficients of the polynomials and the RMS of the surface fit.

The analysis results are presented in Figure 8. The RMS values after the fit are shown in the left panel of the Figure. These results may be characterized as having a large drop in the RMS with the inclusion of the Vertical Astigmatism term that is so obvious in the maps of Figure 7. We find that, beyond the 15th polynomial term, the RMS values tend to reach a steady value of approximately 88 microns. This suggests that the impact of the higher order deformations is small in the LMT system and that, for removal of thermal effects, the most important terms are those below number 15.

On the righthand panel of Figure 8, we show the values of the coefficients for each map. The dominant term is the Vertical Astigmatism term, and it is clear that there are large variations from night to night in the magnitude of the effect.

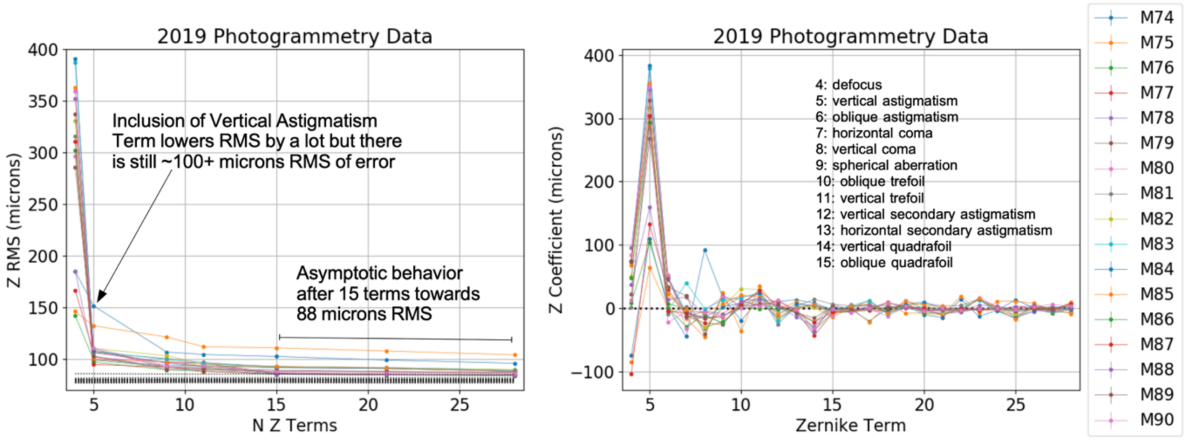

Figure 8. Analysis of the maps presented in Figure 7. For each map the surface is fit to a set of Zernike polynomials. This allows coefficients to be derived along with the surface RMS remaining after each term is removed. The left panel shows the surface RMS for each map as successively higher order terms are removed. We find that removal of the Vertical Astigmatism term (number 5 in our nomenclature) provides a significant reduction in the overall RMS, and that beyond about fifteen Zernike terms, we see only marginal improvement in the surface RMS. The right panel shows the values of the coefficients fit to the maps. It is clear that, beyond simple defocus, the Vertical Astigmatism term is the most important contributor to the deformation, though there is clear systematic behavior in the terms out to number 15.

3.3 Relationship to Thermal Gradients

In order to make a connection between the derived values of Zernike Coefficients in the maps and thermal gradients within the structure, we have attempted to find correlations between these values. By and large, there are few clear correlations between the Zernike coefficients from the fits and temperature gradients within the structure. Figure 9 shows an interesting correlation between the antenna radial temperature gradient and the Vertical Astigmatism deformation of the surface. We are continuing to study relationships like this in order to build a real-time correction model based on the temperature sensor readings - recognizing that this will be the first approach to a broader set of corrections and mitigations. In the meantime, the presence of a relationship is a useful indicator that the deformations observed in our maps are likely to be the result of thermal gradients in the structure.

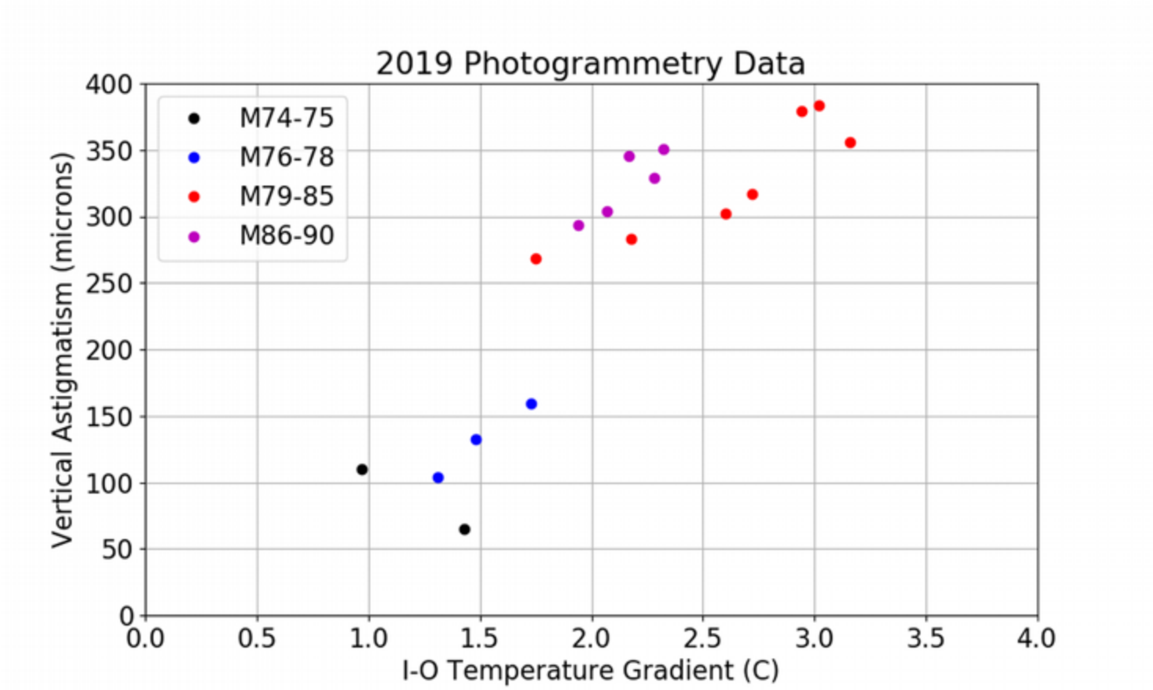

Figure 9. Correlation of the radial temperature gradient in the antenna BUS (I-O) and the best-fit Vertical Astigmatism coefficient in each map.

4. MANAGEMENT AND MEASUREMENT OF THERMAL DISTORTION

In this section, we consider some of the many possible approaches to dealing with deformations caused by thermal gradients within the telescope structure. The LMT's strategy is to pursue all of these approaches as we seek to improve the antenna performance under daytime conditions when solar heating can drive temperature differences within the structure. It is also anticipated that these improvements will improve the performance under nighttime conditions. In addition to minimizing effects of thermal gradients which arise as the structure cools, we also anticipate that the overall setting of the surface segments can be improved now that the thermal deformations present in nighttime maps are better characterized and understood.

4.1 Minimizing Thermal Gradients

The original LMT design called for two measures to be taken to minimize thermal gradients that arise within the structure. The first idea was to cover the structure with insulating cladding in order to slow its rate of temperature change. This cladding system, which is apparent in Figure 1, was implemented during the construction of the telescope. Ideally, if the telescope were only subject to heating and cooling through coupling with the ambient air, then introducing insulation would: (1) reduce the amplitude of daily temperature changes experienced by the structure compared to the temperature changes in the ambient environment; and (2) introduce a phase lag between the daily diurnal air temperature cycle and the temperature of the structural element. The results of our thermal characterization work (see Figure 4) have shown that the cladding does not substantially reduce the range of temperatures compared to the outdoor air temperatures, though it does introduce a phase lag in the diurnal cycle that also depends on the thermal mass of the components. Thermal modelling of the behavior suggests that solar heating of the cladding during daylight hours plays an important role in determining the structural temperatures.

The combination of the LMT's cladding and the thermal mass of the LMT's structures does lead to relatively smooth and simple diurnal temperature changes. Moreover, as shown in Figure 5, the temperature differences between major structural elements are small. Within the BUS, we note that the cladding has an important effect of holding heated air inside the

BUS during the day. This leads to the development of vertical temperature gradients within the BUS as hot air rises to the top of the BUS and is retained by the cladding.

The second concept for the LMT thermal control was to include a system of fans in the BUS to stir the air and minimize temperature differences within the BUS enclosure. As seen in Figure 5, differences of ~2 K can arise during daylight hours across the structure due to uneven solar heating. The nominal LMT system design is based on a similar system at the IRAM 30m telescope[3,4], though it does not attempt to control the structural temperatures to achieve a fixed value. We are in the process of defining the requirements for this system with the goal of acquiring and installing the system within the next one to two years.

4.2 Predicting Deformations from Temperature Measurements

Careful modeling of the structure, using finite element techniques, combined with measurement of the temperatures of the structural components can be used to predict deformations of the antenna surface[5]. The technique has been considered for use on the LMT[6], and results like those shown in Figure 9 represent first steps in this pursuit. Accurate predictions require a relatively large number of temperature sensors on the structure, on the order of 200. The LMT project is in the process of acquiring and installing 256 sensors.

4.3 Direct Astronomical Measurements of Deformations

Measurements of astronomical sources may be used to determine deformations of the antenna surface. For example, the out-of-focus (OOF) holography technique has been employed at some observatories to make routine measurements of the low-order Zernike terms describing the surface of the antenna[7,8]. At the LMT, we have developed a similar technique that makes use of the LMT's active surface to directly measure the principal surface deformation, the Vertical Astigmatism[9]. Figure 10 illustrates the basic principle. The Vertical Astigmatism Zernike polynomial is programmed into the surface with different values for the Zernike coefficient. Then, at each value, a measurement of the signal strength from a strong calibration source is obtained. The response of the antenna peaks at the best value of the coefficient, and when combined with standard refocusing of the antenna, we are able to optimize the antenna gain.

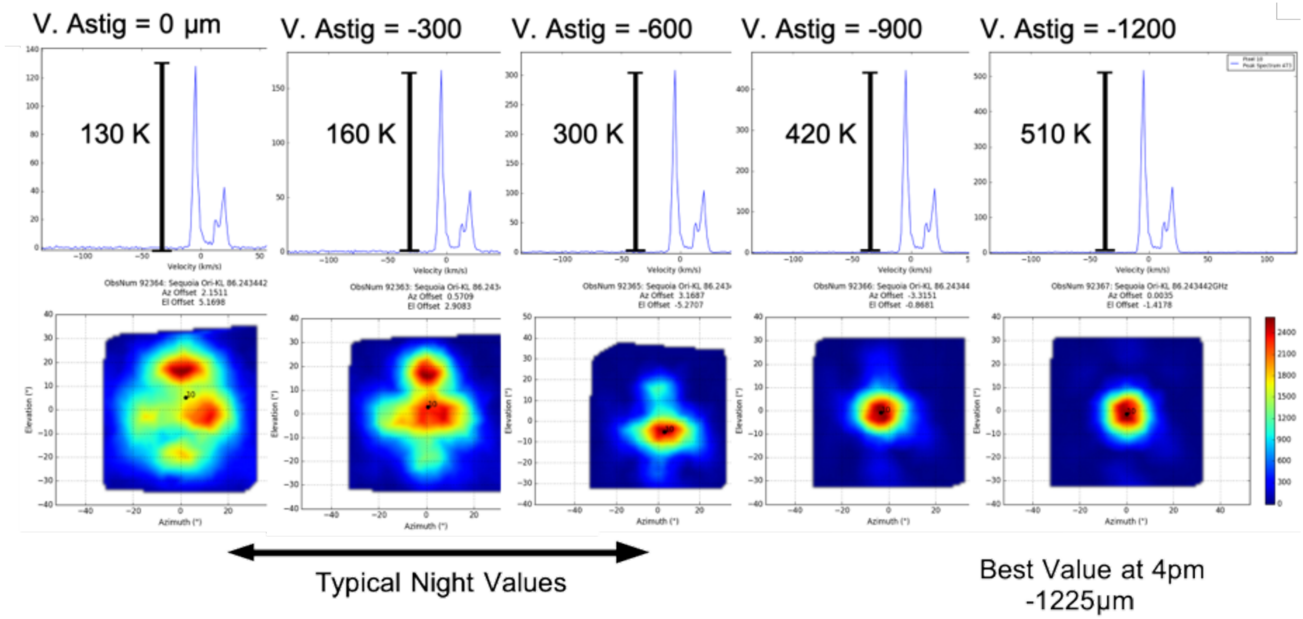

Figure 10. Measuring Vertical Astigmatism on the LMT using its active surface. Measurements of the spectrum of the 86 GHz SiO maser are shown along with maps of the beam pattern. Observations were made during daylight hours at approximately 4pm local time. The best position, with a value of approximately -1200 microns for the Zernike coefficient, is quite significantly different from typical values (-300) observed under nighttime conditions. However, this adjustment recovers nearly all the antenna gain. This technique is a part of the regular LMT observing routine.

The measurement in Figure 10 is notable because it was made during daytime conditions (4 pm local time) at the site. The best value for the coefficient for Vertical Astigmatism (-1225 microns) was found to be several hundred microns different from values obtained under nighttime conditions (~ -300 microns) on the previous night and night following the measurement. However, when the surface correction is applied, the signal strength for the source is fully recovered. Figure 11 shows the results for focus and astigmatism measurements near this time made during nighttime conditions, where the large change in the Vertical Astigmatism is apparent.

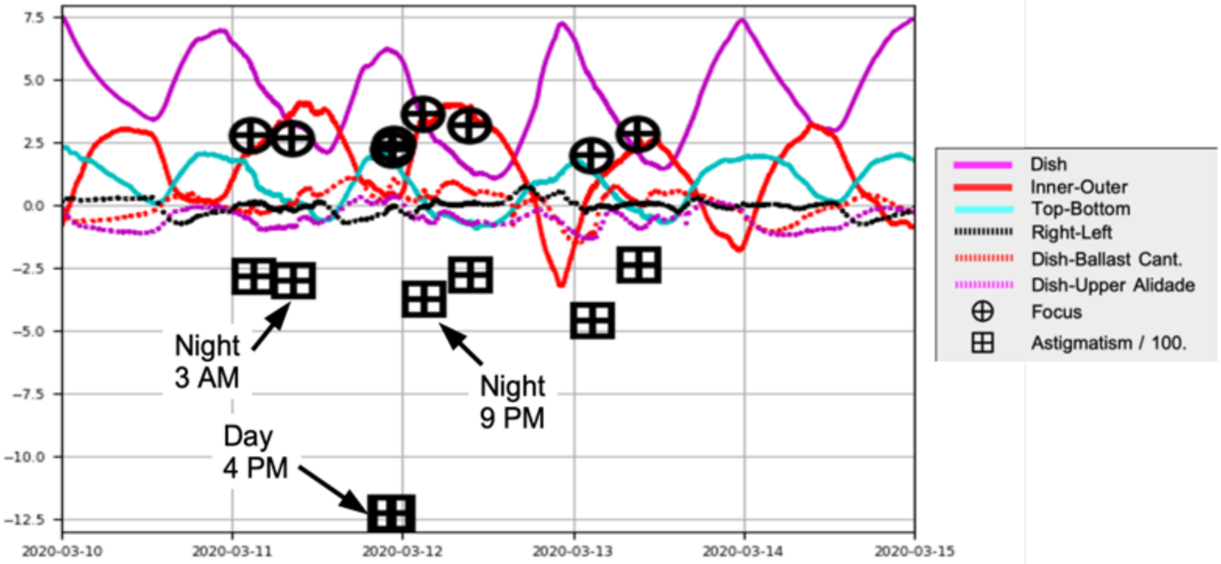

Figure 11. Measurements of Focus and Vertical Astigmatism of the LMT under day and night conditions. The daytime observation is indicated as are the two nighttime observations made closest in time. A large change in the Vertical Astigmatism parameter is observed to occur during the day. The Y axis in the graph is scaled to show temperatures, in degrees C, best focus position in mm, and vertical astigmatism in units of 100 microns.

4.4 Real-time measurement system

Astronomical measurements of surface shape have the disadvantage that they take time away from science observing in order to carry out the measurements. Thus, large telescopes continue to seek a means to make more direct measurements of the surface shape in real-time. One technique involves the use of "Terrestrial Laser Scanner" (TLS) devices, which are capable of scanning over a large target area and producing a point cloud of measurements to map the antenna surface[10,11].

A recent application of this is underway at the Green Bank Telescope[12], with operational use of the system expected to begin sometime in 2021. The off-axis geometry of the Green Bank Telescope lends itself well to the TLS approach, since it is possible to mount the TLS instrument at a point on the structure that does not block the main aperture. For telescopes with more traditional geometries, like the LMT, however, this approach is less desirable. The TLS must be able to view the surface of the antenna, and the obvious positions for the device are in front of the surface where it blocks the aperture. Thus, for the LMT we have been considering alternative concepts.

Another promising real-time measurement approach makes use of a number of precise point-to-point distance measurements on the structure. The concept is described by Rakich *et al*[13] as it has been developed for position measurements of optics in large optical telescopes. Our group has been developing an idea for using this technology to measure the large-scale deformations of the LMT surface in real-time. This concept is presented in the next section.

5. A CONCEPT FOR REAL-TIME MEASUREMENT OF THERMAL DISTORTION ON THE LMT

The Terrestrial Laser Scanner approach, which is currently being pursued at the Green Bank Telescope, offers many positive features for real-time surface measurement. The point cloud that results from the measurement covers the full surface at high resolution and would in principle allow the alignment of individual reflector panels to be identified and corrected. The main difficulty in implementing this technique is the practical one of placing the instrument at a location where it can see the entire surface without blocking the aperture. Previous uses of a TLS at the 100m Effelsberg telescope[10] and the Onsala 20m telescope[11] involved placing the instrument near the subreflector or on one of the subreflector supports. In both cases, for use in regular operation, a portion of the antenna aperture would be blocked by the instrument, and measurements from a single location cannot see the entire surface. Another operational problem, which is very important at the LMT's mountain site, is that of providing appropriate protection for an instrument suspended from the subreflector under poor weather conditions. Therefore, we have sought a new approach to the problem.

Finite Element predictions and direct measurements of the surface at LMT show that thermal deformations of the surface should be of low spatial order. This means that large numbers of measurements are not required to determine deformations we seek to characterize and remove. Therefore, we are investigating the possibility of using precise point-to-point distance measurements within the structure as a way to measure low order deformations in real-time.

To make the measurements, we have been investigating the Etalon Absolute Multiline Technology system[14], which is commercially available from Hexagon DEU01 GmbH – Etalon[15]. This system allows for point-to-point distance measurements on a structure using an interferometric technique. The nominal relative accuracy of the length measurement ($\delta L/L$) is 5 x 10^{-7}.

5.1 Primary Reflector Measurements

The primary mirror of the LMT is subject to deformation in response to thermal gradients within the antenna structure. Our study of the shapes of these deformations indicates that they may be removed with measurement of coefficients of 15 Zernike polynomials, and so a real-time system needs to be able to determine the contribution of each polynomial coefficient with a minimum amount of crosstalk with the other coefficients. Figure 12 illustrates one approach that appears to satisfy the basic needs. A system of 16 point-to-point distance measurements is used to solve for the coefficients of the lowest order Zernike polynomials. We find, in simulations of the system installed at various locations on the surface, that radial distance measurements are much more sensitive to the Zernike polynomials than measurements between points at the same radius. We also find best results when all points are placed on the parabola being measured rather than having one end on a separate structure not connected to the surface.

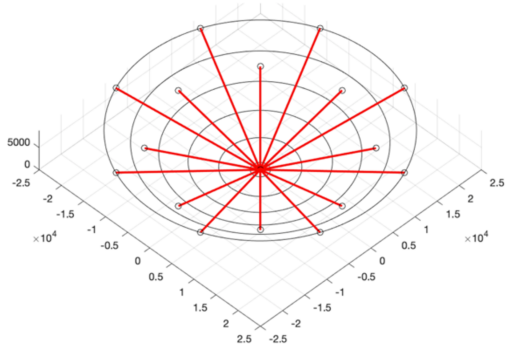

Figure 12. Distribution of 16 point-to-point measurements on the LMT primary reflector surface. For simplicity, all points originate at the primary vertex which is considered to be part of the parabola.

A Monte Carlo simulation of the measurement experiment was performed using the sixteen measurements to determine 14 Zernike polynomial coefficients. (The constant term, Z_0, cannot be found through measurement of relative positions

on the parabola.) The simulation was made assuming that the relative measurement error is *ten times* the nominal value, corresponding to $5x10^{-6}$. A "corner plot" of the errors in the simulations is shown in Figure 13. Errors for each Zernike coefficient are tabulated in Table 1 for the nominal relative measurement error of $5x10^{-7}$.

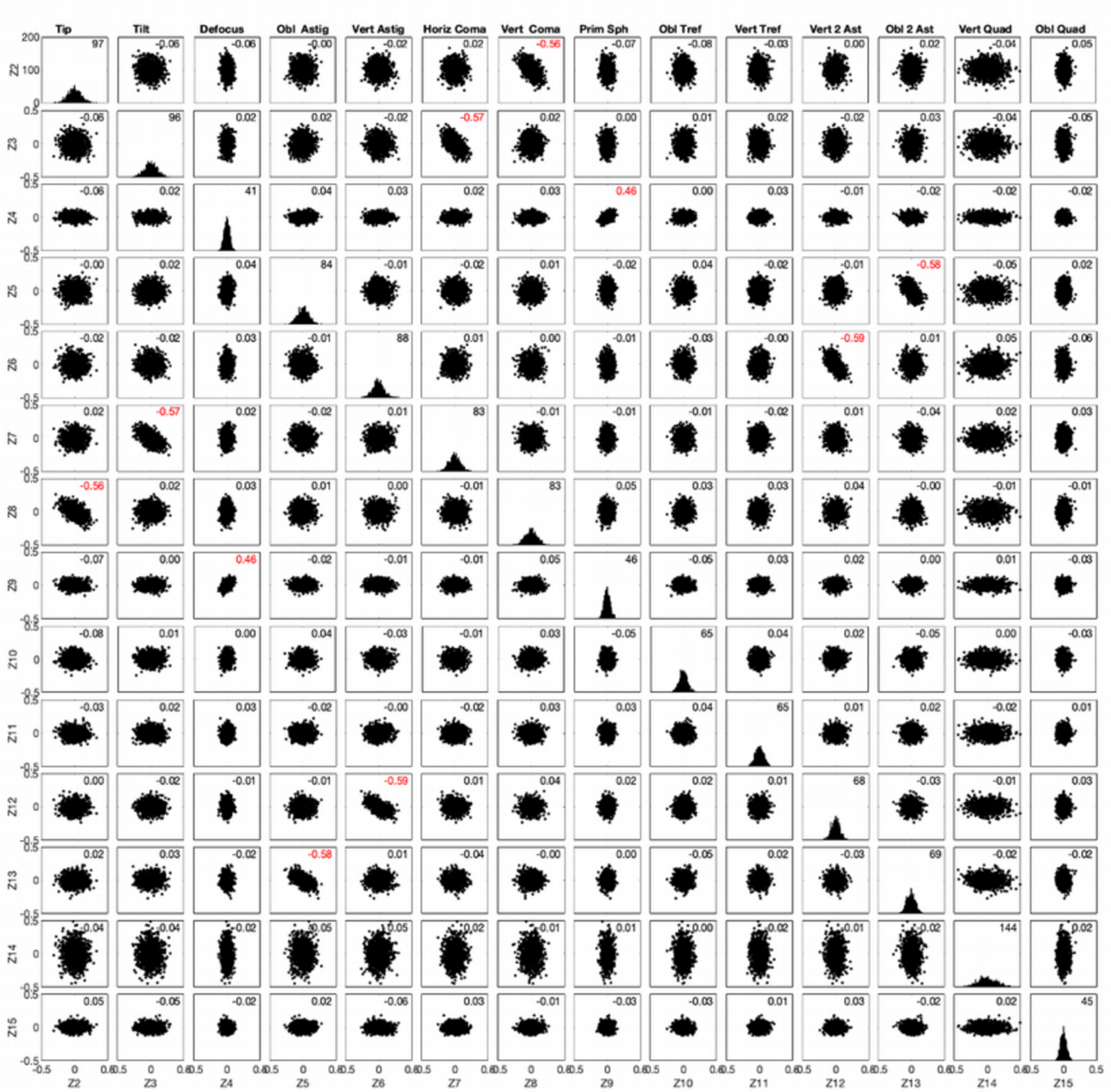

Figure 13. A corner plot showing the results of Monte Carlo simulation of the experiment to determine 14 Zernike coefficients. (The fifteenth is the constant term and cannot be determined from relative position measurements within the parabola.) The Monte Carlo simulation assumed relative measurement errors of 5 x 10^{-6} which is *ten times* the nominal value. The diagonal across the figure shows histograms of the errors for coefficient, with the standard deviation of the error presented in the upper right corner of the plot in units of microns. The off-diagonal figures show the correlated errors from the simulation for each parameter pair. Here the number in the upper right corner of the figure is the correlation coefficient between parameters. Five cases of values in excess of 0.1 are highlighted in red. All windows are scaled to show errors in the range -0.5 to +0.5 mm.

We find that the important Zernike polynomial coefficients may be determined to an error level of a few microns, meaning that if the shape is removed by the LMT's active surface, the residual surface RMS error will be approximately 30 microns.

TABLE 1

Surface Zernike Terms	Error (microns)
Tip	9.7
Tilt	9.6
Defocus	4.1
Vertical Astigmatism	8.4
Oblique Astigmatism	8.8
Horizontal Coma	8.3
Vertical Coma	8.3
Primary Spherical	4.6
Oblique Trefoil	6.5
Vertical Trefoil	6.5
Vertical Secondary Astigmatism	6.8
Oblique Secondary Astigmatism	6.9
Vertical Quadrafoil	14.4
Oblique Quadrafoil	4.5
Surface RMS Reconstruction	30.3

5.2 Secondary Position Measurements

One of the major temperature differences within the antenna structure occurs between the secondary mirror support legs (the tetrapod) and the other structural elements of the antenna. Relative positioning of the secondary mirror is critical to the overall performance of the telescope. Lateral errors in secondary position at the level of 100 microns result in pointing errors of approximately 0.8 arcsec. Errors in secondary position along the optical axis of the parabola lead to decrease in gain, with a position error of 100 microns resulting in a 1% gain decrease at a wavelength of 1.3mm. Thus, for work at its shortest wavelengths, it is important for LMT to position the secondary mirror with high accuracy.

Figure 14 illustrates the concept for determination of the position of the secondary mirror with respect to the primary. A set of eight point-to-point measurements are made between a location at the base of each tetrapod leg and points attached to the LMT secondary mirror. The points on the secondary mirror can be simple retroreflector targets, which simplifies the implementation of the system. The total of eight measurements is used to determine the location and orientation in space with respect to the reference points on the surface. Thus, we have 8 measurements and 6 degrees of freedom (three translational and three rotational) to be constrained. We have carried out a Monte Carlo simulation of the measurement process using the nominal relative distance errors of the system. Errors of several microns are found for the translational degrees of freedom; errors on the determination of the rotational angles are at the arcsecond level.

Given the simulated results, one can compute the expected antenna properties that would result. Z errors in the secondary position at the level of 11 microns RMS have no effect on the antenna gain, and so the impact on performance is mainly through pointing effects. The X-Y translation errors at the level of 8 microns lead to pointing errors of 0.07 arcsec. The X-Y tilt errors of 2 arcsec lead to 0.16 arcsec pointing errors. If all errors are combined the final RMS pointing error (due to this term in the pointing error budget) would be 0.25 arcsec. An antenna pointing error of this amount means that the beam peak is not on the source and the received power is reduced by 0.5%

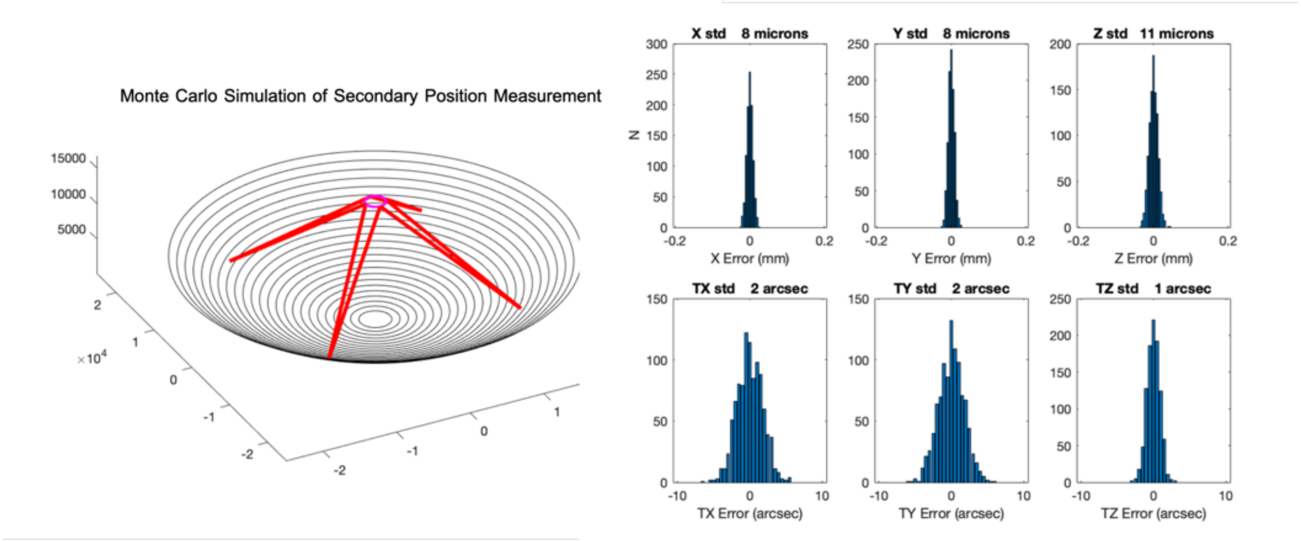

Figure 14. Approach to measurement of the LMT secondary position. (left) Arrangement of point-to-point measurements between locations on the LMT surface and positions at the edge of the secondary mirror. Beams originate at the primary surface near the base of the tetrapod legs. Passive retroreflectors are then placed on the secondary. A system of 8 measurements is used to solve for the six degrees of freedom that are required to locate the secondary mirror in space relative to the surface reference points. (right) Results of Monte Carlo simulation of the measurement experiment, displayed as histograms of the errors for each of the six degrees of freedom. We note that translational motions are determined to the 10-micron RMS level. Rotations are measured to the level of ~2 arcseconds RMS.

5.3 System Implementation

Etalon Absolute Multiline Technology system[14,15] offers several useful features for the practical implementation of the metrology system we have described above. A distance measurement involves placement of a laser beam collimator and a retroreflector on the antenna structure. The retroreflector is a passive device, and so may be placed in positions (such as at the secondary mirror position) that would be difficult to access. The collimator end of a measurement is fed by optical fibers from a central unit which may be located away from the devices on the surface. Therefore, the fibers can be easily routed from an environmentally controlled location to the surface location where they are required. A feature of the Absolute Multiline Technology system is that it allows transmission of the beam through vacuum windows. We are in the process of developing a design for the LMT that can be mounted on the antenna surface and secondary mirror and sealed behind windows to protect its optical elements against the weather conditions at the LMT site. In summary, we find that these operational advantages and general lack of moving parts in the system, offer significant advantages over approaches making use of terrestrial laser scanners.

6. CONCLUSION

The LMT Collaboration has collected a significant amount of data to characterize the thermal behavior of the antenna and the response of the structure to temperature gradients. The information gathered is useful both to our pursuit of scientific observations in daytime conditions and also to our program of aligning the antenna surface in order to improve the overall surface accuracy of the dish. The team is poised to advance towards daytime observing through a number of measures, including installation of an active ventilation system for the antenna backup structure, improvement in predictions of thermal deformation based on correlation of temperature measurements with deformation measurements, real-time measurement of thermal deformation using astronomical observations, and real-time measurements of surface deformation using a new technique now under development. We look forward to achieving one of the original LMT design goals, which called for use of active measurement systems and the active antenna surface to achieve stable performance under a wide range of thermal conditions.

ACKNOWLEDGEMENTS

We acknowledge the effort of the LMT photogrammetry team: Maribel Lucero Álvarez, Esteban Tecuapetla Sosa, David Castro Santos, Carlos Tzile Torres, and Emilio Hernández Rios. The Large Millimeter Telescope project is grateful for the sustained support of the Consejo Nacional de Ciencia y Tecnología (CONACyT) and the Fondo Institucional de Fomento Regional para el Desarrollo Científico, Tecnológico y de Innovación (FORDECYT) program. FPS also acknowledges the Next Generation Event Horizon Telescope Design Project (NSF AST-1935980) for support of his efforts devoted to LMT thermal characterization, thermal modeling, and the development of real-time measurement concepts.

REFERENCES

[1] Zeballos, M., Ferrusca, D., Contreras R., J., Hughes, D. H. "Reporting the first 3 years of 225-GHz opacity measurements at the site of the Large Millimeter Telescope Alfonso Serrano," Proc. SPIE 9906, Ground-based and Airborne Telescopes VI, 99064U (2016)

[2] Gale, D.M., Schloerb, F.P., León Huerta, A., Lucero Álvarez, M., Cabrera Cuevas, L., Tecuapetla Sosa, E., Castro Santos, D., Tzile Torres, C., Hernández Rios, E., "Photogrammetry mapping and alignment of the LMT 50-meter primary reflector," Proc. SPIE 10706, Advances in Optical and Mechanical Technologies for Telescopes and Instrumentation III, 1070646 (2018)

[3] Baars, J.W.M., Greve, A., Hooghoudt, B.G., and Penalver, J. "Thermal control of the IRAM 30-m millimeter radio telescope" Astron. Astrophys., 195 364-371 (1988).

[4] Greve, A., Dan, M., and Penalver, J., "Thermal Behavior of Millimeter Wavelength Radio Telescopes" IEEE Transactions on Antennas and Propagation, 40, 1375-1388 (1992)

[5] Greve, A., Bremer, M., Peñalver, J., Raffin, P., and Morris, D. "Improvement of the IRAM 30-m Telescope From Temperature Measurements and Finite-Element Calculations" IEEE TRANSACTIONS ON ANTENNAS AND PROPAGATION, 53, 851-860 (2005)

[6] Antebi, J., Kan, F.W., and Rao, R.S. "Active segmented primary reflector and pointing accuracy of the Large Millimeter Telescope (LMT)", Proc. SPIE 3357, Advanced Technology MMW, Radio, and Terahertz Telescopes, (1998)

[7] Nikolic, B., Hills, R. E., and Richer, J. S. "Measurement of antenna surfaces from in- and out-of-focus beam maps using astronomical sources" A&A 465, 679–683 (2007)

[8] Nikolic, B., Prestage, R. M., Balser1, D. S., Chandler, C. J., and Hills, R. E. "Out-of-focus holography at the Green Bank Telescope", A&A 465, 685–693 (2007)

[9] Schloerb, F. P.; Sanchez, D.; Narayanan, G.; Erickson, N.; Souccar, K.; Wilson, G.; Gale, D.; Hughes, David H.; Smith, D., "Calibration and operation of the active surface of the Large Millimeter Telescope", Proceedings of the SPIE, Volume 9906, id. 99066C, 7 pp. (2016).

[10] Holst, C. and Kuhlmann, H. "Aiming at self-calibration of terrestrial laser scanners using only one single object and one single scan" Journal of Applied Geodesy 8(4): 295–310 (2014)

[11] Holst, C., Schunck, D., Nothnagel, A., Haas, R., Wennerbäck, L., Olofsson, H., Hammargren, R. and Kuhlmann, H. "Terrestrial Laser Scanner Two-Face Measurements for Analyzing the Elevation-Dependent Deformation of the Onsala Space Observatory 20-m Radio Telescope's Main Reflector in a Bundle Adjustment" Sensors 17, 1833 (2017)

[12] Salas, P.; Marganian, P.; Seymour, A.; Brandt, J.; Egan, D.; Jensen, L.; Sizemore, N.; Bloss, M.; Beaudet, C.; Schwab, F.; Lockman, F. "LASSI: keeping the Green Bank Telescope in shape" American Astronomical Society meeting #235, id. 175.16. Bulletin of the American Astronomical Society, Vol. 52, No. 1 (2020)

[13] Rakich, A., Dettmann, Lee, Leveque, S., Guisard, S. “A 3-D metrology system for the GMT” in Ground-based and Airborne Telescopes VI, edited by Helen J. Hall, Roberto Gilmozzi, Heather K. Marshall, Proc. of SPIE Vol. 9906, 990614 · (2016)

[14] Dale, J., Hughes, B., Lancaster, A.J., Lewis, A.J., Reichold, A.J.H. and Warden, M.S. “Multi-channel absolute distance measurement system with sub-ppm-accuracy and 20 m range using frequency scanning interferometry and gas absorption cells”, Optics Express, Vol. 22, 24869-24893 (2014)

[15] https://www.etalonproducts.com/en/products/absolute-multiline-technology/ (2020)